Available online at www.sciencedirect.com
ScienceDirect
Journal of Sound and Vibration 315 (2008) 536–555
JOURNAL OF SOUND AND VIBRATION
www.elsevier.com/locate/jsvi

Periodic geometrically nonlinear free vibrations of circular plates

S. Stoykov[a,b], P. Ribeiro[b,*]

[a]*Faculty of Mathematics and Informatics, Sofia University "St. Kliment Ohridski", 5 James Bourchier Blvd., 1164 Sofia, Bulgaria*
[b]*IDMEC/DEMEGI, Faculdade de Engenharia, Universidade de Porto, R. Dr. Roberto Frias, s/n, 4200-465 Porto, Portugal*

Accepted 4 February 2008
The peer review of this article was organised by the Guest Editor
Available online 14 March 2008

Abstract

The geometrically nonlinear free vibrations of thin isotropic circular plates are investigated using a multi-degree-of-freedom model, which is based on thin plate theory and on Von Kármán's nonlinear strain–displacement relations. The middle plane in-plane displacements are included in the formulation and the common axisymmetry restriction is not imposed. The equations of motion are derived by the principle of the virtual work and an approximated model is achieved by assuming that the in-plane and transverse displacement fields are given by weighted series of spatial functions. These spatial functions are based on hierarchical sets of polynomials, which have been successfully used in *p*-version finite elements for beams and rectangular plates, and on trigonometric functions. Employing the harmonic balance method, the differential equations of motion are converted into a nonlinear algebraic form and then solved by a continuation method. Convergence with the number of shape functions and of harmonics is analysed. The numerical results obtained are presented and compared with available published results; it is shown that the hierarchical sets of functions provide good results with a small number of degrees of freedom. Internal resonances are found and the ensuing multimodal oscillations are described.

1. Introduction

Thin plate structures are encountered in various modern engineering problems and they are often subjected to severe dynamic loading, which may result in large vibration amplitudes, inducing significant geometrical nonlinearities. This leads to well-known consequences, as a change of the resonance frequencies and of the mode shapes with the amplitude of vibration. Moreover, the natural frequencies may become commensurable creating conditions for the strong interaction of the natural modes involved. As a result of this phenomenon, known as internal resonance, energy is interchanged between those modes and the response becomes multimodal [1].

One of the plate geometries of interest in engineering is circular and the nonlinear vibrations of circular plates have been studied by several authors in the past decades. In the following sentences a brief, thus incomplete, review is carried out. In Ref. [2] Sridhar et al. studied the axisymmetric response of a circular plate

*Corresponding author. Tel.: +351 22 508 17 16; fax: +351 22 508 14 45.
E-mail address: pmleal@fe.up.pt (P. Ribeiro).

0022-460X/$ - see front matter © 2008 Elsevier Ltd. All rights reserved.
doi:10.1016/j.jsv.2008.02.001

to a harmonic excitation. The method of multiple scales was employed and internal resonances were found. Hadian and Nayfeh [3] used the method of multiple scales to investigate the axisymmetric response of circular plates in the case of internal resonance. A reduced model based on specifically chosen mode shapes was employed. Liu and Chen [4] analysed the geometrically nonlinear free vibrations of polar orthotropic circular plates using an axisymmetric finite element method. Haterbouch and Benamar [5–8] carried out rather complete investigations on the harmonic and axisymmetric nonlinear vibrations of circular plates; the equations of motion were derived from the kinetic and potential energies and the harmonic balance method was employed with one harmonic. While in Refs. [2–8] thin plate theory was followed, in Ref. [9] Raju and Rao employed the finite element method to compute the first nonlinear natural frequencies in axisymmetric vibrations of circular plates and to investigate the effect of shear deformation and rotary inertia. The authors concluded that the hardening spring effect is stronger in thick plates. Sathyamoorthy [10] investigated the influence of transverse shear and rotary inertia on the nonlinear vibrations of circular plates, assuming that the transverse displacement is defined by a single axisymmetric mode. As in Ref. [9], a stronger hardening spring effect took place in thicker plates.

The studies referred to in the previous paragraph and a few more are devoted to axisymmetric vibrations. Some, but much fewer, studies were also carried out in asymmetric vibrations. By asymmetric we mean that the deformed shape is not symmetric with respect to the central axis. Sridhar et al. [11] used the method of multiple scales to investigate asymmetric vibrations. According to Yeo and Lee the solvability conditions derived in the former reference are not correct, and other conditions were presented in Ref. [12]. The same authors investigated the asymmetric vibrations of a clamped circular plate on an elastic foundation [13]. Touzé et al. [14] carried out an interesting study of the forced asymmetric nonlinear vibrations of circular plates with a free edge expressing the deflection as a function of linear modes. This study was followed by an experimental investigation in Ref. [15]. In all these studies not restricted to axisymmetric vibrations, the perturbation method of multiple scales was employed.

The use of hierarchical basis functions on geometrically nonlinear vibrations of beams and rectangular plates has been found to be very efficient and allows employing multi-degree-of-freedom models with flexibility and a reasonable computational cost (see Refs. [16–21] for example). The harmonic balance method (HBM) and continuation method also proved to give important information in beams and rectangular plates [18–20]. Although the HBM has some drawbacks, it also has some advantages when compared to perturbation methods, like the method of multiple scales. The most important advantages are that it is not restricted to small amplitude vibrations and its use with multi-degree-of-freedom models is relatively simple. The objective of this paper is to analyse the geometrically nonlinear free vibrations of clamped immovable thin circular plates using for the first time the above-mentioned methods. We intend to investigate the variation of the mode shapes with the vibration amplitude and to study internal resonances. There are several studies on axisymmetric vibrations of circular plates (Refs. [2–10] and others) and internal resonances may possibly relate axisymmetric and asymmetric modes. Therefore, the present model is not limited to axisymmetric modes. If the plates are thin, Von Kármán large deflection theory provides a good approximation and thus it will be employed here.

2. Formulation

Consider a circular plate of thin uniform thickness h and radius R that is clamped along its edge. The cylindrical coordinate is chosen such that the middle plane (i.e. $z = 0$) of the plate coincides with the $r\theta$-plane. The origin of the coordinate system is at the centre of the plate with the z-axis pointing downward in the thickness direction (Fig. 1). The plate material is assumed to be elastic, homogeneous and isotropic.

The displacements (u_r, u_θ, u_z) are functions of time and of the r, θ and z coordinates. We begin with the following displacement field from the classical plate theory:

$$u_r(r,\theta,z,t) = u_r^0(r,\theta,t) - z\frac{\partial u_z^0}{\partial r}, \quad u_\theta = (r,\theta,z,t) = u_\theta^0(r,\theta,t) - z\left(\frac{1}{r}\frac{\partial u_z^0}{\partial \theta}\right),$$
$$u_z(r,\theta,z,t) = u_z^0(r,\theta,t), \tag{1}$$

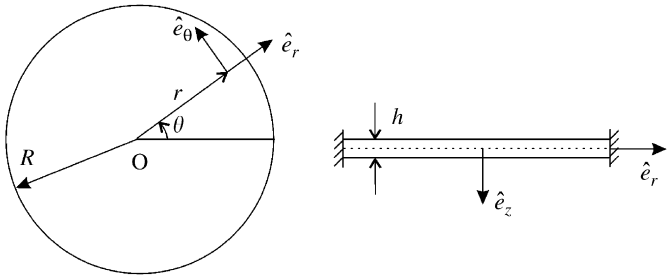

Fig. 1. Clamped circular plate.

where $(u_r^0, u_\theta^0, u_z^0)$ are the displacements in the radial, circumferential and transverse directions, respectively, of a point on the middle plane of the plate. The displacement field (1) is based on Kirchhoff hypothesis. From now on the superscript 0 will be dropped, as displacements will always be those of the middle surface. In this paper, we will use bold for matrices and column vectors except when necessary to discriminate the components of the array, in which case we will use: [] for matrices, {} for column vectors and ⌊⌋ for row vectors. It is also noted that function arguments are often not written, for example, we may write u_r instead of $u_r(r, \theta, z, t)$.

The middle plane displacements are expressed in the form

$$\begin{Bmatrix} u_r(\xi,\eta,t) \\ u_\theta(\xi,\eta,t) \\ u_z(\xi,\eta,t) \end{Bmatrix} = \begin{bmatrix} \mathbf{N}^{r^{\mathrm{T}}}(\xi,\eta) & 0 & 0 \\ 0 & \mathbf{N}^{\theta^{\mathrm{T}}}(\xi,\eta) & 0 \\ 0 & 0 & \mathbf{N}^{z^{\mathrm{T}}}(\xi,\eta) \end{bmatrix} \begin{Bmatrix} \mathbf{q}_r(t) \\ \mathbf{q}_\theta(t) \\ \mathbf{q}_z(t) \end{Bmatrix}. \tag{2}$$

The row vectors of bi-dimensional shape functions are

$$\mathbf{N}^{r^{\mathrm{T}}}(\xi,\eta) = \left\lfloor g_1(\xi)gt_1(\eta) \quad g_1(\xi)gt_2(\eta)\ldots g_{p_i}(\xi)gt_{p_i}(\eta) \right\rfloor = \left\lfloor N_1^r(\xi,\eta) \quad N_2^r(\xi,\eta)\ldots N_{p_i^2}^r(\xi,\eta) \right\rfloor, \tag{3}$$

$$\mathbf{N}^{\theta^{\mathrm{T}}}(\xi,\eta) = \left\lfloor h_1(\xi)ht_1(\eta) \quad h_1(\xi)ht_2(\eta)\ldots h_{p_i}(\xi)ht_{p_i}(\eta) \right\rfloor = \left\lfloor N_1^\theta(\xi,\eta) \quad N_2^\theta(\xi,\eta)\ldots N_{p_i^2}^\theta(\xi,\eta) \right\rfloor, \tag{4}$$

$$\mathbf{N}^{z^{\mathrm{T}}}(\xi,\eta) = \left\lfloor f_1(\xi)ft_1(\eta) \quad f_1(\xi)ft_2(\eta)\ldots f_{p_o}(\xi)ft_{p_o}(\eta) \right\rfloor = \left\lfloor N_1^z(\xi,\eta) \quad N_I^z(\xi,\eta)\ldots N_{p_o^2}^z(\xi,\eta) \right\rfloor, \tag{5}$$

where p_o and p_i are the numbers of one-dimensional out-of-plane and in-plane shape functions, respectively; **g** and **gt** are the vectors of in-plane radial shape functions; **h** and **ht** are the vectors of in-plane circumferential shape functions; **f** and **ft** are vectors of out-of-plane shape functions; and $\mathbf{q}_r$, $\mathbf{q}_\theta$ and $\mathbf{q}_z$ are the two in-plane and one out-of-plane generalized displacement vectors. Shape functions **gt**, **ht** and **ft** are in the circumferential direction and the others are in the radial direction. The set of shape functions in the radial direction is based on a set of polynomials employed in Refs. [16–21], but with the argument varying from 0 to 1. Trigonometric functions [22] are used as shape functions in the circumferential direction. Appendix A gives the one-dimensional shape functions and shows plots of some of them. The dimensionless coordinates ξ and η are given by

$$\xi = r/R, \quad 0 \leqslant \xi \leqslant 1, \qquad \eta = \theta/\pi, \quad -1 \leqslant \eta \leqslant 1. \tag{6}$$

The sets of polynomials employed in Refs. [16–21] were chosen as shape functions in the radial direction because they have a number of well-proven advantages, some of which are: it is easy to define higher order sets for improved approximations where the polynomials corresponding to lower approximations constitute a subset, all polynomials possess both a zero value (displacement) and a zero derivative (slope) at each boundary, they result in models with a small number of degrees of freedom (dof), they are not prone to ill-conditioning, and the computational effort required to define the elemental matrices is reduced.

Trigonometric sets of functions and one constant function, which also has to be included in order to obtain all the axisymmetric modes, are used as shape functions in the circumferential direction. Travelling waves have been found in circular plates with axisymmetric boundary conditions [12–14], where a pair of companion asymmetric modes appears. The two members of each pair share the same natural frequency but their shapes are rotated at an angle of $\pi/(2\text{nd})$, nd being the number of nodal diameters. However, in this first study we will only investigate standing waves and therefore, simple sets with either sine or cosine terms will be employed as circumferential shape functions, i.e., we do not include the rotated shapes.

Von Kármán's nonlinear strain–displacement relationships are expressed as

$$\begin{Bmatrix} \varepsilon_r \\ \varepsilon_\theta \\ \gamma_{r\theta} \end{Bmatrix} = \begin{bmatrix} 1 & 0 & 0 & z & 0 & 0 \\ 0 & 1 & 0 & 0 & z & 0 \\ 0 & 0 & 1 & 0 & 0 & z \end{bmatrix} \boldsymbol{\varepsilon}, \tag{7}$$

where

$$\boldsymbol{\varepsilon} = \begin{Bmatrix} \boldsymbol{\varepsilon}_0^p \\ \boldsymbol{\varepsilon}_0^b \end{Bmatrix} + \begin{Bmatrix} \boldsymbol{\varepsilon}_L^p \\ 0 \end{Bmatrix}. \tag{8}$$

The linear membrane and bending strains, $\boldsymbol{\varepsilon}_0^p$ and $\boldsymbol{\varepsilon}_0^b$, and the geometrically nonlinear membrane strain, $\boldsymbol{\varepsilon}_L^p$, are defined as

$$\boldsymbol{\varepsilon}_0^p = \begin{Bmatrix} \dfrac{\partial u_r}{\partial r} \\ \dfrac{1}{r}u_r + \dfrac{1}{r}\dfrac{\partial u_\theta}{\partial \theta} \\ \dfrac{1}{r}\dfrac{\partial u_r}{\partial \theta} + \dfrac{\partial u_\theta}{\partial r} - \dfrac{u_\theta}{r} \end{Bmatrix}, \quad \boldsymbol{\varepsilon}_0^b = \begin{Bmatrix} -\dfrac{\partial^2 u_z}{\partial r^2} \\ -\dfrac{1}{r}\left(\dfrac{\partial u_z}{\partial r} + \dfrac{1}{r}\dfrac{\partial^2 u_z}{\partial \theta^2}\right) \\ -\dfrac{2}{r}\left(\dfrac{\partial^2 u_z}{\partial r \partial \theta} - \dfrac{1}{r}\dfrac{\partial u_z}{\partial \theta}\right) \end{Bmatrix}, \quad \boldsymbol{\varepsilon}_L^p = \begin{Bmatrix} \dfrac{1}{2}\left(\dfrac{\partial u_z}{\partial r}\right)^2 \\ \dfrac{1}{2r^2}\left(\dfrac{\partial u_z}{\partial \theta}\right)^2 \\ \dfrac{1}{r}\dfrac{\partial u_z}{\partial r}\dfrac{\partial u_z}{\partial \theta} \end{Bmatrix}. \tag{9}$$

The equations of motion are derived by applying the principle of the virtual work. Using the constitutive relations of the plate, and in the absence of external forces, one obtains

$$\int_\Omega (\delta \boldsymbol{\varepsilon}_0^{p\mathrm{T}} + \delta \boldsymbol{\varepsilon}_L^{p\mathrm{T}}) \mathbf{A} (\boldsymbol{\varepsilon}_0^p + \boldsymbol{\varepsilon}_L^p)\, \mathrm{d}\Omega + \int_\Omega \delta \boldsymbol{\varepsilon}_0^{b\mathrm{T}} \mathbf{D}\, \boldsymbol{\varepsilon}_0^b\, \mathrm{d}\Omega + \rho h \int_\Omega (\delta u_r \ddot{u}_r + \delta u_\theta \ddot{u}_\theta + \delta u_z \ddot{u}_z)\, \mathrm{d}\Omega = 0, \tag{10}$$

where ρ denotes mass per unit volume and Ω the area of the plate. $\mathbf{A}$ and $\mathbf{D}$ are the membrane and flexural rigidity matrices, given by

$$\mathbf{A} = \frac{Eh}{1-\nu^2} \begin{bmatrix} 1 & \nu & 0 \\ \nu & 1 & 0 \\ 0 & 0 & \dfrac{1-\nu}{2} \end{bmatrix}, \quad \mathbf{D} = \frac{h^2}{12}\mathbf{A}, \tag{11}$$

where E represents Young's modulus and ν Poisson's ratio.

Substituting Eq. (9) into Eq. (10) and because the virtual displacements are arbitrary, we obtain

$$\begin{bmatrix} \mathbf{M}_p & 0 \\ 0 & \mathbf{M}_b \end{bmatrix} \begin{Bmatrix} \ddot{\mathbf{q}}_p \\ \ddot{\mathbf{q}}_z \end{Bmatrix} + \left(\begin{bmatrix} \mathbf{K}_{1p} & \mathbf{0} \\ \mathbf{0} & \mathbf{K}_{1b} \end{bmatrix} + \begin{bmatrix} \mathbf{0} & \mathbf{K}_2(\mathbf{q}_z) \\ \mathbf{0} & \mathbf{0} \end{bmatrix} + \begin{bmatrix} \mathbf{0} & \mathbf{0} \\ \mathbf{K}_3(\mathbf{q}_z) & \mathbf{0} \end{bmatrix} + \begin{bmatrix} \mathbf{0} & \mathbf{0} \\ \mathbf{0} & \mathbf{K}_4(\mathbf{q}_z) \end{bmatrix} \right) \begin{Bmatrix} \mathbf{q}_p \\ \mathbf{q}_z \end{Bmatrix} = \begin{Bmatrix} \mathbf{0} \\ \mathbf{0} \end{Bmatrix}. \tag{12}$$

In the former equation $\mathbf{q}_p$ is the vector of generalized in-plane displacements, defined as $\mathbf{q}_p^{\mathrm{T}} = \begin{bmatrix} \mathbf{q}_r^{\mathrm{T}} & \mathbf{q}_\theta^{\mathrm{T}} \end{bmatrix}$; $\mathbf{M}_p$ and $\mathbf{M}_b$ are the in-plane and bending inertia matrices; $\mathbf{K}_{1p}$ and $\mathbf{K}_{1b}$ are the in-plane and bending stiffness matrices; and $\mathbf{K}_2(\mathbf{q}_z)$, $\mathbf{K}_3(\mathbf{q}_z)$ and $\mathbf{K}_4(\mathbf{q}_z)$ represent the nonlinear stiffness matrices. These matrices are defined in Appendix B.

Neglecting the in-plane inertia and eliminating $\mathbf{q}_p$ results in the following equations of motion:

$$\mathbf{M}_b \ddot{\mathbf{q}}_z + \mathbf{K}_{1b}\mathbf{q}_z + \mathbf{K}_{n\ell}(\mathbf{q}_z)\mathbf{q}_z = 0, \tag{13}$$

where the nonlinear stiffness matrix, which is a quadratic function of the generalized transverse displacements $\mathbf{q}_z$, is defined as

$$\mathbf{K}_{n\ell}(\mathbf{q}_z) = \mathbf{K}_4(\mathbf{q}_z) - 2\mathbf{K}_2(\mathbf{q}_z)^{\mathrm{T}}\mathbf{K}_{1p}\mathbf{K}_2(\mathbf{q}_z). \tag{14}$$

In the former equation relation $\mathbf{K}_3 = 2\mathbf{K}_2^{\mathrm{T}}$, which is obtained by comparing the form of $\mathbf{K}_2$ and $\mathbf{K}_3$, was used.

Only periodic motions about the equilibrium position $\mathbf{q}_z = \mathbf{0}$ will be analysed and the nonlinearity is cubic; in this case $\mathbf{q}_z$ may be expressed as

$$\mathbf{q}_z(t) = \sum_{i=1}^{k} \mathbf{w}_{2i-1} \cos((2i-1)\omega t), \tag{15}$$

i.e. only odd harmonics are considered in Eq. (15). With the former expression only standing waves can be investigated. As we stated before, travelling waves may appear due to the co-existence of pairs of companion modes with the same number of nodal diameters [12–14]. To analyse travelling waves, $\sin((2i–1)\omega t)$ terms should be inserted into Eq. (15), and "sin" and "cosine" sets of trigonometric functions should be used as shape functions in the circumferential direction. A preliminary analysis indicates that the methods employed here also allow one to investigate travelling waves, but we will only investigate standing waves.

Inserting Eq. (15) into the equations of motion (13) and applying the HBM, the equations of motion in the frequency domain are derived. These are of the form

$$\mathbf{F}(\mathbf{w}, \omega^2) = (-\omega^2\mathbf{M} + \mathbf{K}_L + \mathbf{K}_{\mathrm{NL}}(\mathbf{w}))\mathbf{w} = \mathbf{0}, \tag{16}$$

where $\mathbf{M}$ represents the mass matrix, $\mathbf{K}_L$ the linear stiffness matrix and $\mathbf{K}_{\mathbf{NL}}(\mathbf{w})$ the nonlinear stiffness matrix, which depends quadratically on the vector of generalized displacements $\mathbf{w}$. The latter is given by

$$\mathbf{w} = \begin{Bmatrix} \mathbf{w}_1 \\ \mathbf{w}_3 \\ \vdots \\ \mathbf{w}_{2k-1} \end{Bmatrix}. \tag{17}$$

The frequency domain equations of motion when three odd harmonics are considered are explicitly given in Appendix C.

The total number of dof of the model is $n = kp_o^2$, where k is the number of terms considered in Eq. (15). The equations of motion are solved by a continuation method which was used, for example, in Refs. [18–20] and which is based on the method presented in Refs. [23,24]. The method is composed of two main loops: in the external loop a predictor to the solution is defined and this is corrected in the internal loop. The continuation parameter is the arc-length and therefore it is possible to pass turning points.

Finally, the transverse displacement is obtained by inserting $\mathbf{q}_z$ from Eq. (15) into Eq. (2)

$$u_z(\xi, \eta, t) = \sum_{i=1}^{k} \mathbf{N}^z(\xi, \eta)^{\mathrm{T}}\mathbf{w}_{2i-1} \cos((2i-1)\omega t). \tag{18}$$

3. Applications

The geometric properties of the clamped plate analysed are $R = 1\,\mathrm{m}$ and $h = 0.0012\,\mathrm{m}$. The material properties are $E = 2.1 \times 10^{11}\,\mathrm{N\,m^{-2}}$, $\rho = 7800\,\mathrm{kg\,m^{-3}}$, and $v = 0.3$. The plate's linear mode shapes are shown in Fig. 2.

3.1. Analysis of convergence

It is intended to demonstrate that an accurate model can be constructed with a small number of dof with the hierarchical set of functions employed here. Therefore, the convergence with the number of harmonics and with the number of shape functions is discussed in the following paragraphs.

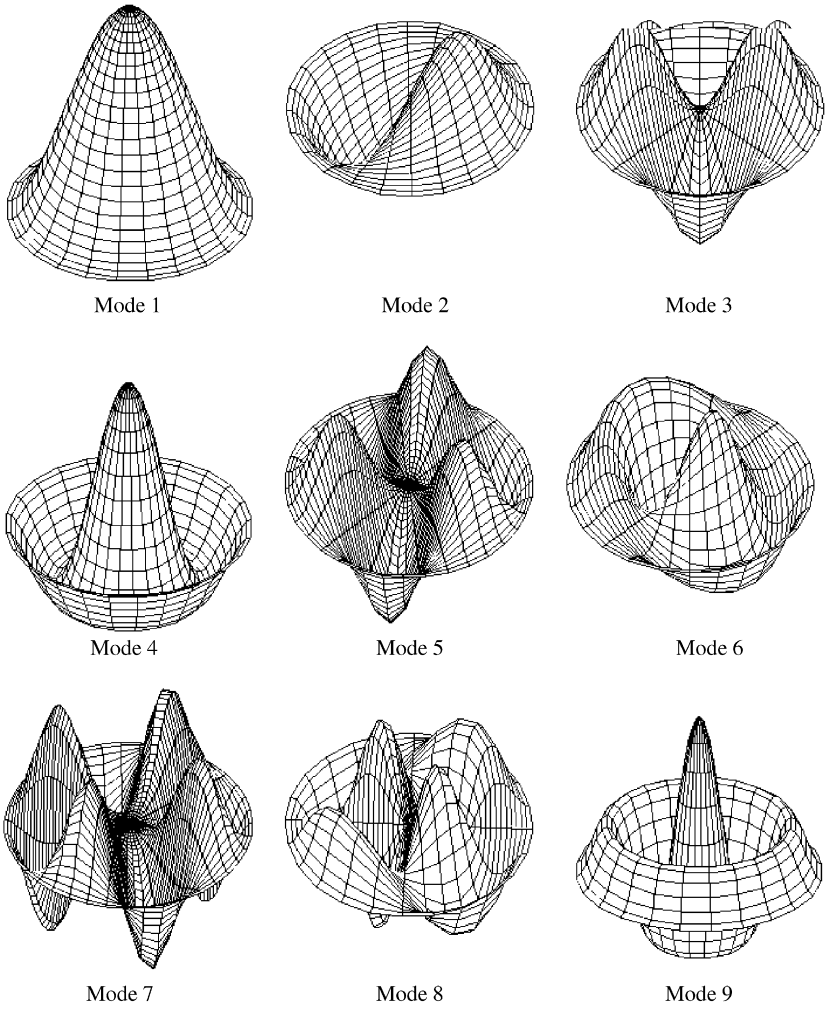

Fig. 2. First nine linear mode shapes, $p_o = 10$.

Table 1
Dimensionless linear natural frequencies, given by $\lambda = \omega R^2\sqrt{\rho h/D}$, where $D = Eh^3/12(1-\nu)$

Number of shape functions dof	3 9	5 25	7 49	9 81	Ref. [25]
λ_{l1}	10.22	10.22	10.22	10.22	10.22
λ_{l2}	21.31	21.26	21.26	21.26	21.26
λ_{l3}	36.45	34.89	34.88	34.88	34.88
λ_{l4}	42.56	39.79	39.77	39.77	39.77
λ_{l5}	63.41	51.05	51.03	51.03	51.04
λ_{l6}		60.94	60.83	60.83	60.82
λ_{l7}		69.94	69.67	69.67	69.67
λ_{l8}		85.46	84.59	84.58	84.58
λ_{l9}		89.94	89.11	89.10	89.10
λ_{l10}			90.76	90.74	90.74

Table 1 shows the convergence of the linear natural frequencies with the number of out-of-plane shape functions. The values are compared with the ones published by Leissa [25]. Five out-of-plane shape functions (25 dof) give a very good approximation to the first nine linear frequencies and with nine out-of-plane shape

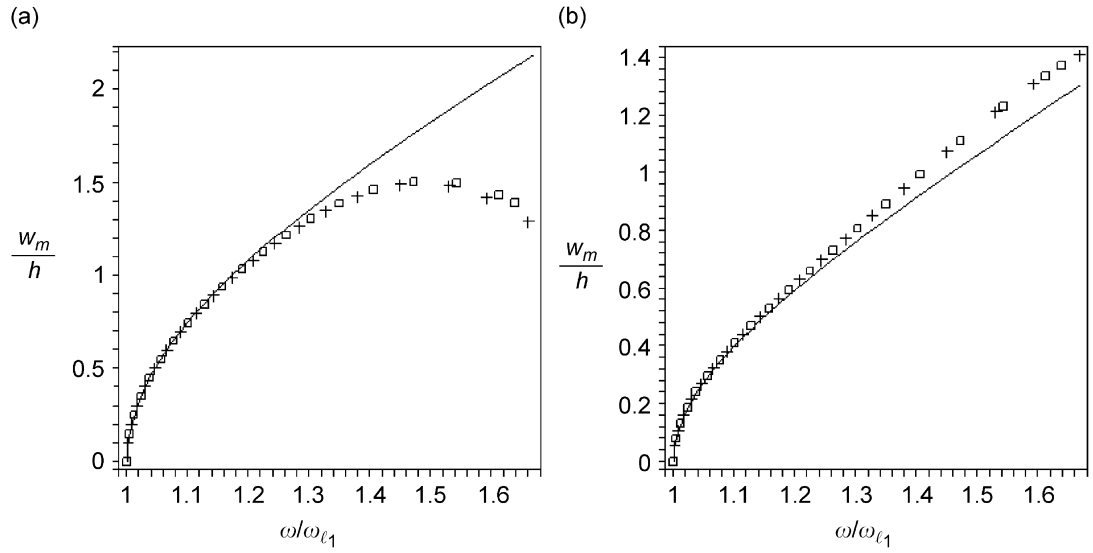

Fig. 3. Total amplitude of vibration displacement at $t = 0$ s: (a) $(\xi, \eta) = (0, 0)$, (b) $(\xi, \eta) = (0.5, 0.5)$; (—) one harmonic, (□) two harmonics, and (+) three harmonics ($p_o = 5$, $p_i = 9$).

functions (81 dof) the first 10 linear frequencies are calculated precisely. The linear natural frequencies are obtained by solving the eigenvalue problem that is the linear version of Eq. (16). The corresponding linear mode shapes, shown in Fig. 2, are obtained be replacing the eigenvectors in Eq. (2).

Fig. 3 compares the amplitude of vibration displacement at point (ξ, η) and $t = 0$ s, computed using one, two and three harmonics. This means that w_m is given by

$$w_m = \mathbf{N}^z(\eta, \xi)^{\mathrm{T}} \sum_{i=1}^{k} \mathbf{w}_{2i-1}, \tag{19}$$

where k represents the number of harmonics. It is recalled that only odd harmonics are considered and that, therefore, the first harmonic corresponds to the first term in the expansion of $\mathbf{q}_z$ (Eq. (15)), the third harmonic to the second term and the fifth harmonic to the third term.

Fig. 3 demonstrates that the one harmonic approximation is only accurate for moderate amplitudes of vibration. The importance of the fifth harmonic slightly increases with ω/ω_{ℓ_1}, but the expansion with the first and third harmonics gives a very reasonable approximation in the frequency span of the figures and is very accurate for amplitudes of the order of the plate's thickness. Consequently, these two harmonics will be used in the following analysis.

Fig. 4 indicates that the backbone curve is accurately calculated with $p_o = 5$. W_1 and W_3 represent, respectively, the amplitudes of the first and third harmonics given by

$$W_1(\eta, \xi) = \mathbf{N}^z(\eta, \xi)^{\mathrm{T}} \mathbf{w}_1, \quad W_3(\eta, \xi) = \mathbf{N}^z(\eta, \xi)^{\mathrm{T}} \mathbf{w}_3. \tag{20}$$

The amplitude of the first harmonic is calculated at $(\xi, \eta) = (0, 0)$ where the largest amplitude of vibration of the first mode is achieved; the amplitude of the third harmonic is calculated at $(\xi, \eta) = (0.41, 0.5)$, where mode 4 has a large vibration amplitude (Fig. 2).

Fig. 5 shows that eight in-plane shape functions are enough to accurately approximate the backbone curves of the first and third harmonics. Due to the condensation implemented to obtain Eq. (13), the number of in-plane shape functions does not interfere with the final number of dof; therefore, we will use nine in-plane shape functions in the model.

Table 2 compares the ratios of the first nonlinear frequency to the first linear frequency with the ratios published in Ref. [7]. It can be seen that the results of the present work agree with the ones obtained by Haterbouch and Benamar, particularly for lower vibration amplitudes. We should note that only one

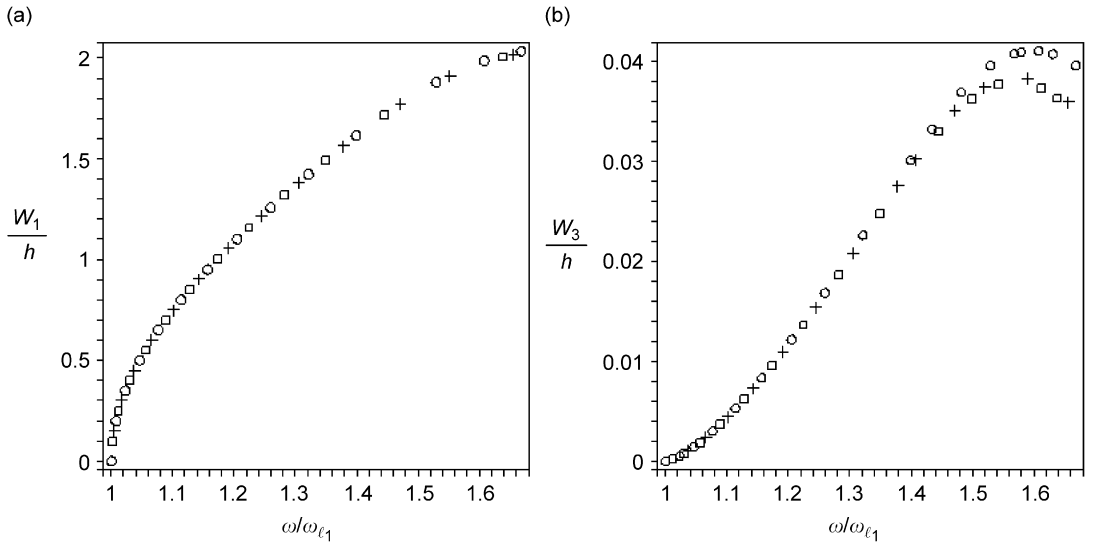

Fig. 4. Amplitude of the first and third harmonics with $p_i = 9$ and: (○) $p_o = 4$, (□) $p_o = 5$, (+) $p_o = 6$: (a) first harmonic at $(\xi, \eta) = (0, 0)$ and (b) third harmonic at $(\xi, \eta) = (0.41, 0.5)$.

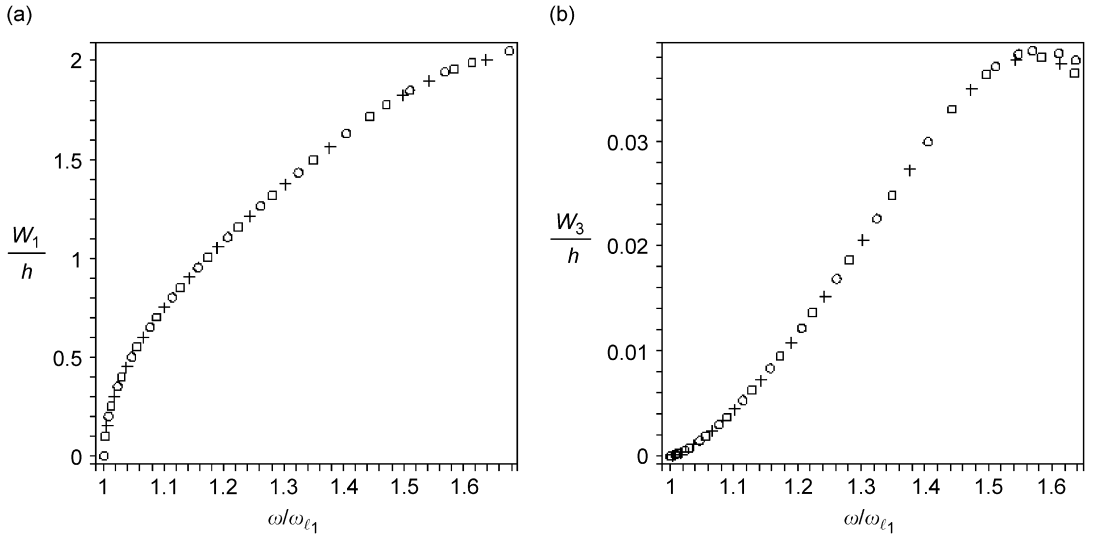

Fig. 5. Amplitude of the first and third harmonics with $p_o = 5$: (○) $p_i = 6$, (□) $p_i = 8$, and (+) $p_i = 9$: (a) first harmonic at $(\xi, \eta) = (0, 0)$ and (b) third harmonic at $(\xi, \eta) = (0.41, 0.5)$.

Table 2
Ratio between the first nonlinear frequency and the first linear frequency

w_m	0.2	0.4	0.6	0.8	1.0	1.5	2.0
Ref. [7]	1.0075	1.0296	1.0654	1.1135	1.1724	1.3568	1.5790
Total shape	1.0075	1.0297	1.0659	1.1154	1.1777	1.4574	–
First harmonic	1.0075	1.0297	1.0654	1.1134	1.1717	1.3512	1.6296

w_m—amplitude of vibration at point $(\xi, \eta) = (0, 0)$ and at $t = 0$ s, $p_o = 5$, $p_i = 9$.

harmonic is employed in Ref. [7] and this is the reason why our values diverge from the ones of that reference at larger amplitudes.

3.2. Bifurcation diagrams and internal resonances

In the following paragraphs, the free vibrations of the plate are studied. Taking into consideration the former convergence studies, a model with two harmonics (first and third), five out-of-plane shape functions and nine in-plane shape functions, i.e. a total of 50 dof, is used.

To analyse the free vibrations we will first trace the backbone curves, which relate the frequency with the vibration amplitude. A branch of solutions is designated as 'main branch' if it contains one solution that cumulatively satisfies the following conditions: occurs at a linear natural frequency or at a linear natural frequency divided by an integer, occurs at zero vibration amplitude, and corresponds to a shape of vibration equal to a linear mode shape. A branch of solutions that bifurcates from a main branch will be designated as 'secondary branch'. We designate as 'bifurcation points' the points where two branches with distinct tangents intersect.

Solving Eq. (16), eigenvalues and eigenvectors are obtained and, from these, a pair frequency/shape that represents the free vibration of the undamped circular plate. We can distinguish three cases. In the first one there is no internal resonance, that is, only one mode is important in the motion and only one vector $\mathbf{w}_i$ is different from zero. In this case, an approximation to the true nonlinear mode shape was computed, but, unlike what happens in reality, the shape does not change during a given periodic motion. The second possible case is the one where there is still no internal resonance, but two vectors $\mathbf{w}_i$ are different from zero. It is easy to see from Eq. (16) that in this case the present model results in a shape that changes during a specified motion, i.e., the shape is not "self-similar at all times" [26]. In both these cases we will say that we obtained an approximation to a nonlinear mode of vibration. Finally, we have the case of internal resonance where two modes are coupled [1].

When a figure caption contains a statement like "bifurcation diagram of the first mode", it should be understood that one of the solutions that is present in that bifurcation diagram corresponds to the first linear mode of vibration; however, more than one mode may be present in solutions in the nonlinear regime.

In Figs. 6 and 7 the bifurcation diagrams of the plate are shown. These diagrams were defined by starting the continuation procedure at the first linear mode. Two main branches were found and in each of them a bifurcation point, which occurs due to a 1:3 internal resonance. A secondary branch links the main branches

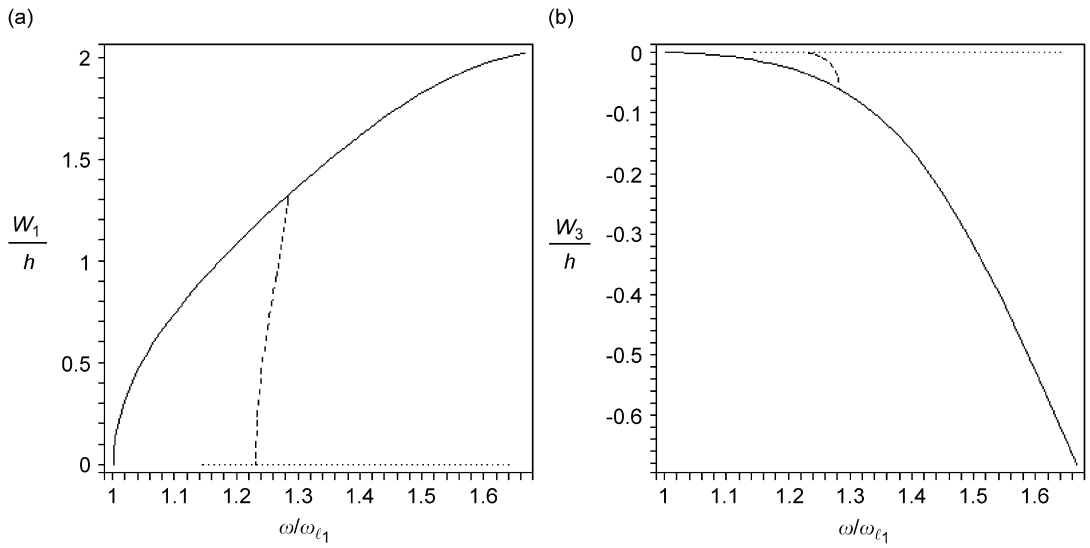

Fig. 6. Bifurcation diagram of the first mode at $(\xi, \eta) = (0, 0)$: (—) first main branch, (- - - -) secondary branch, (···) second main branch; (a) first harmonic and (b) third harmonic.

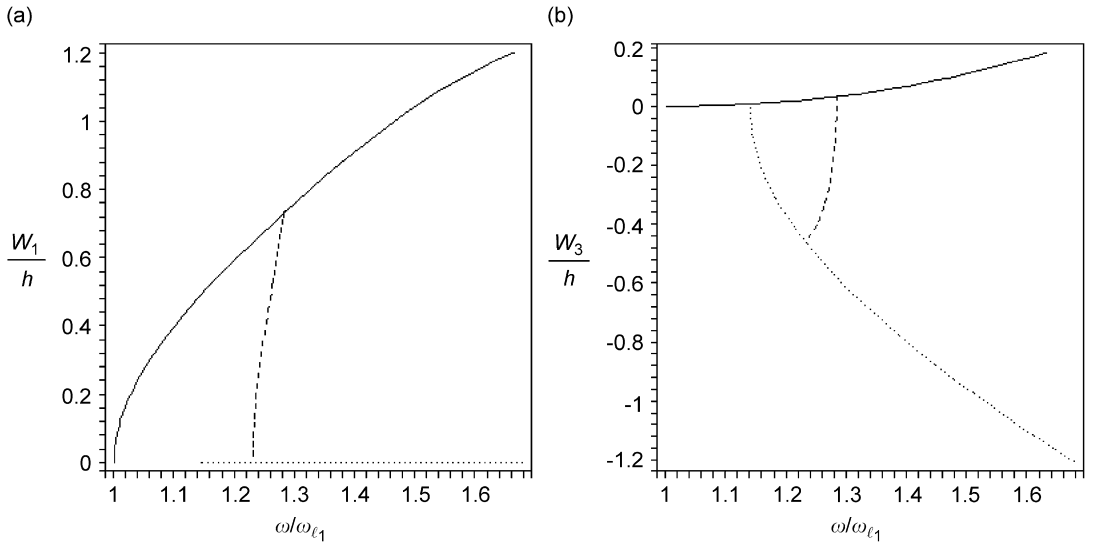

Fig. 7. Bifurcation diagram of the first mode at $(\xi, \eta) = (0.5, 0.25)$: (—) first main branch, (- - -) secondary branch, (···) second main branch; (a) first harmonic and (b) third harmonic.

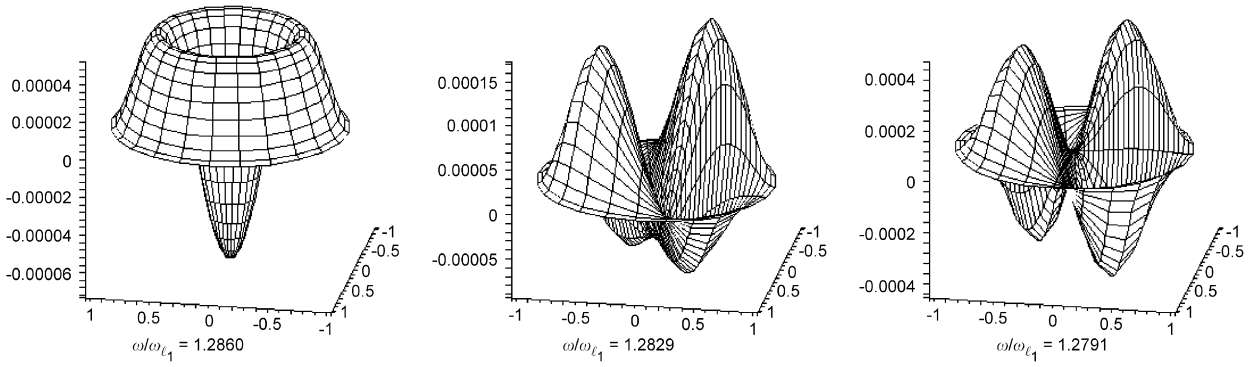

Fig. 8. Transformation of the shape of the third harmonic of the secondary branch moving from the bifurcation point of the first main branch to the bifurcation point of the second main branch.

between these two bifurcation points. The first main branch is born at the first linear mode and it is mainly defined by the first harmonic. Although the shapes of the first harmonic of solutions in the first main branch change with the amplitude, they remain very similar to the first linear mode shape shown in Fig. 2. The second main branch is related to the third mode of vibration and to the third harmonic. This branch starts at the third linear frequency divided by three and with a shape equal to the third linear mode shape. The shape also changes with the amplitude of vibration, but remains quite similar to the shape of the third linear mode.

The secondary branch that links the two bifurcation points involves mainly the first and third modes and the first and third harmonics. As one moves along the secondary branch, from the bifurcation point of the first main branch to the bifurcation point of the second main branch, the importance of the first harmonic decreases while the importance of the third harmonic increases. Also, the shape of the third harmonic transforms from a shape similar to the fourth linear mode—with a very small amplitude—to a shape similar to the third linear mode. These transformations are shown in Fig. 8. The brief appearance of the fourth mode is explained below; the third mode is excited due to a 1:3 internal resonance, since $3\omega \cong \omega_{n\ell_3}$, where ω is the frequency of the fundamental harmonic ($i = 1$ in Eq. (15)).

For most solutions on the secondary branch, the shape of the plate changes considerably during the period of vibration, because it is described by a sum of the first and third modes and involves both harmonics.

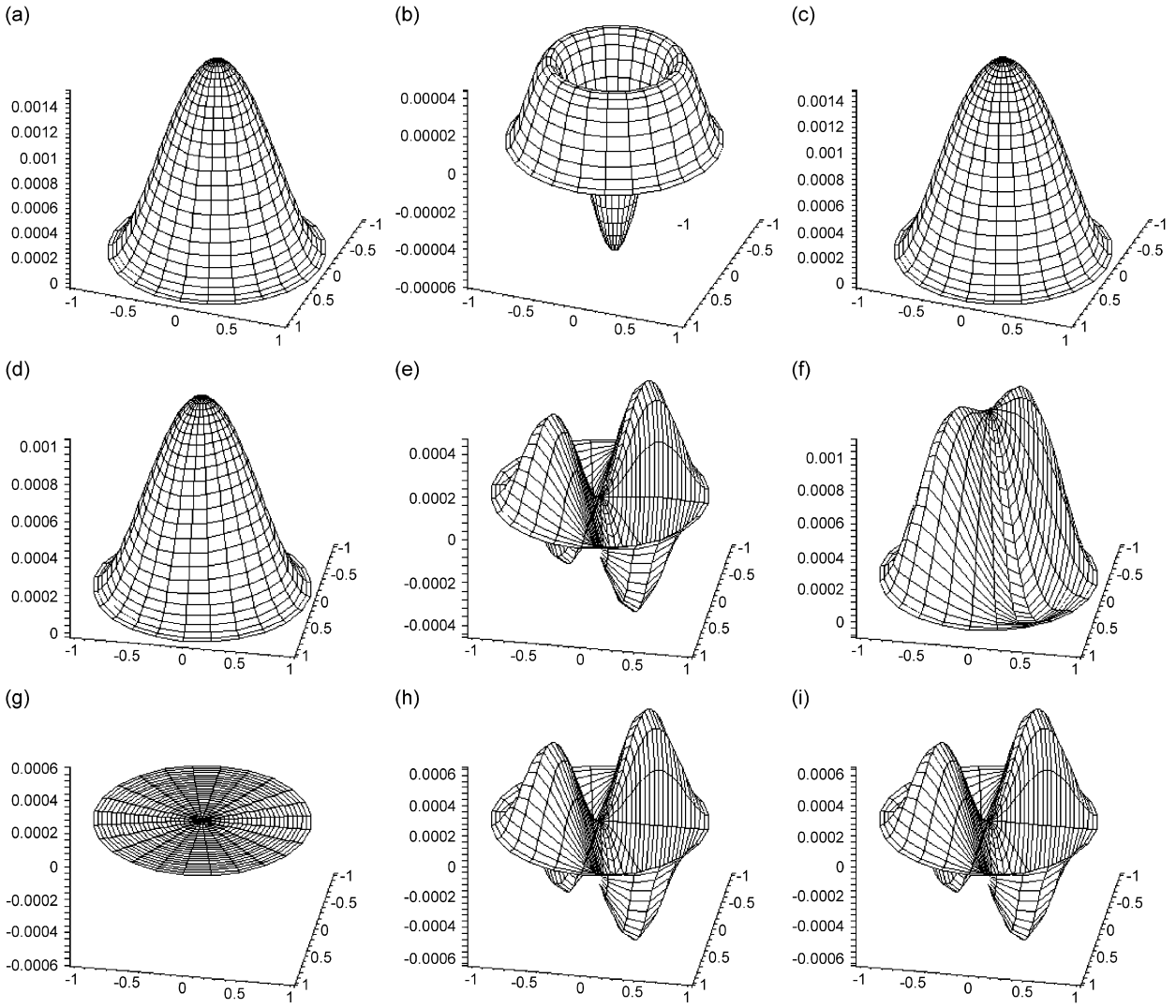

Fig. 9. Shapes of solutions on the three branches at frequency $\omega/\omega_{\ell_1} = 1.26$. First main branch: first harmonic (a), third harmonic (b) and total shape at $t = 0$ s (c). Secondary branch: first harmonic (d), third harmonic (e) and total shape at $t = 0$ s (f). Second main branch: first harmonic (g), third harmonic (h) and total shape at $t = 0$ s (i).

The shapes of the first and third harmonics and the total shape of vibration at $t = 0$ s, of a particular solution on the secondary branch, are shown in Figs. 9(d)–(f), as an example. Fig. 9 also shows the shapes that correspond to solutions at the same frequency but on other branches; the fact that different vibration modes appear on different branches is obvious.

Returning to the first main branch, Fig. 10 shows that after $\omega/\omega_{\ell_1} \cong 1.15$, the importance of the third harmonic increases significantly, a phenomenon that is also due to a 1:3 internal resonance. Fig. 11 shows the shapes assumed by the first and third harmonics for a particular point of the first main branch. The first shape is similar to the first linear mode and the second to mode four; this explains the previously detected appearance of mode four in the beginning of the secondary branch. Both modes are axisymmetric and in this case the internal resonance does not result in a bifurcation point of the backbone curve. Fig. 11(c) shows the total shape of vibration, where the influence of the higher mode is visible. However, because both modes involved are axisymmetric and because the first harmonic is dominant, the influence of the higher mode on the shape is not as noticeable as in the previous example of internal resonance on the secondary branch.

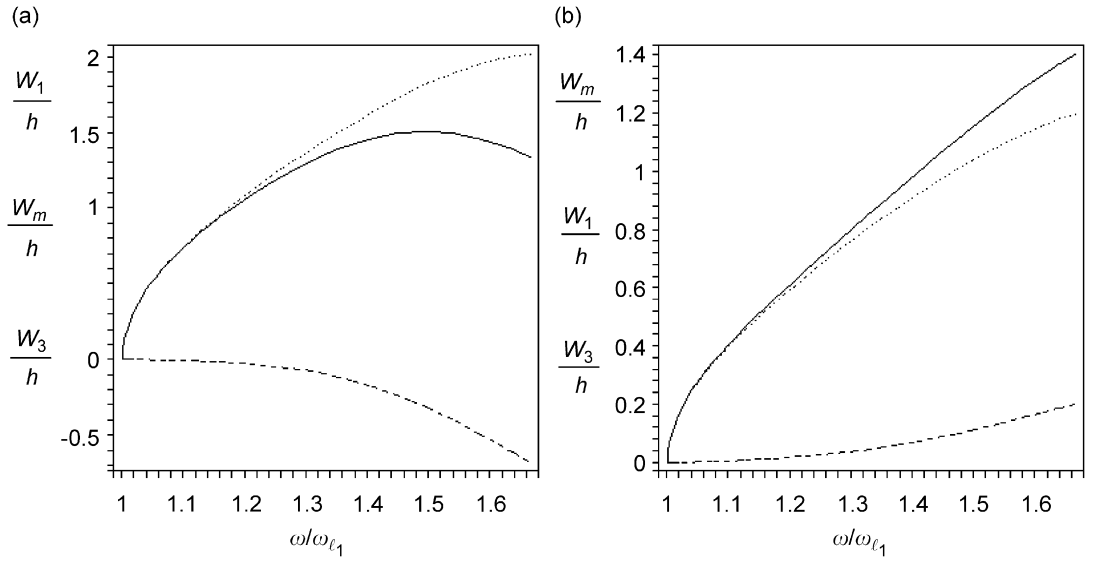

Fig. 10. First main branch: (—) total amplitude at $t = 0$ s (w_m/h), (···) amplitude of the first harmonic (W_1/h), (- - -) amplitude of the third harmonic (W_3/h): (a) $(\xi, \eta) = (0, 0)$ and (b) $(\xi, \eta) = (0.5, 0.25)$.

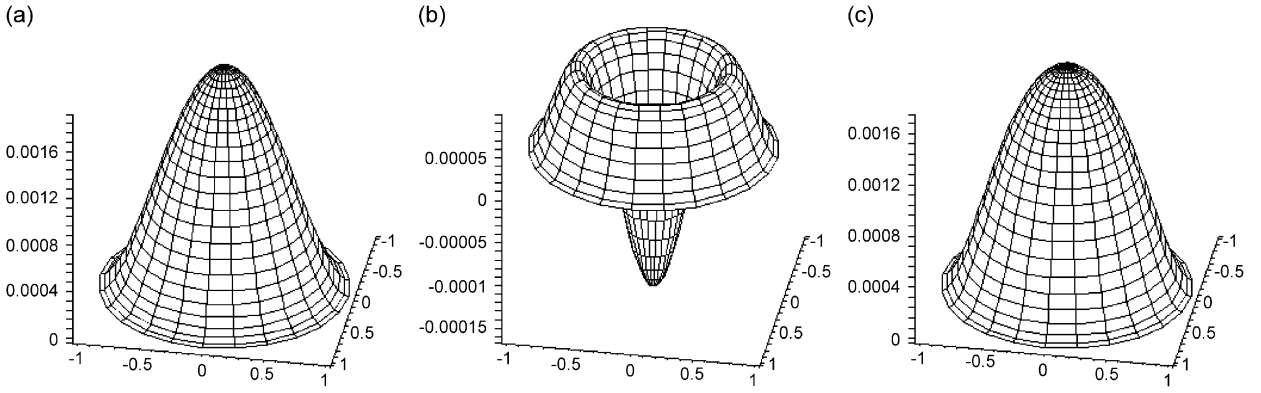

Fig. 11. Shapes at point $\omega/\omega_{\ell_1} = 1.37$ of the first main branch of: (a) first harmonic; (b) third harmonic; and (c) total shape of vibration at $t = 0$ s.

Figs. 12(a) and (b) show sections, at $\eta = 0$, of the shape associated with the first and third harmonics for different points of the first main branch. It is evident that the shapes associated with each harmonic vary with the frequency of vibration, which is equivalent to stating that they vary with the maximum amplitude of vibration, due to the effect of the membrane forces. The variation of the first harmonic shape is very small. Fig. 12(c) represents the shape of the plate defined by both harmonics at $t = 0$ s. This shape varies with the maximum amplitude of vibration displacement, i.e. with the frequency of vibration, because the shapes of each harmonic and the relative weight of each of them vary.

Similar modal coupling and bifurcation phenomena occur in the second mode of vibration. Figs. 13 and 14 represent the bifurcation diagrams of the second mode of the plate. Again, there are two main branches and a secondary branch, which occurs due to a 1:3 internal resonance and links the main branches between two bifurcation points. The internal resonance and bifurcation point on the first main branch occur because $3\omega \cong \omega_{n\ell_7}$ and $\omega = \omega_{n\ell_2}$, where ω is the frequency of the fundamental harmonic. The amplitudes of the figures are computed at $(\xi, \eta) = (0.41, 0.5)$, because here the first harmonic of the first main branch has a large value, and at $(\xi, \eta) = (0.64, 0.875)$, because the third harmonic of the second main branch has a large value at this point.

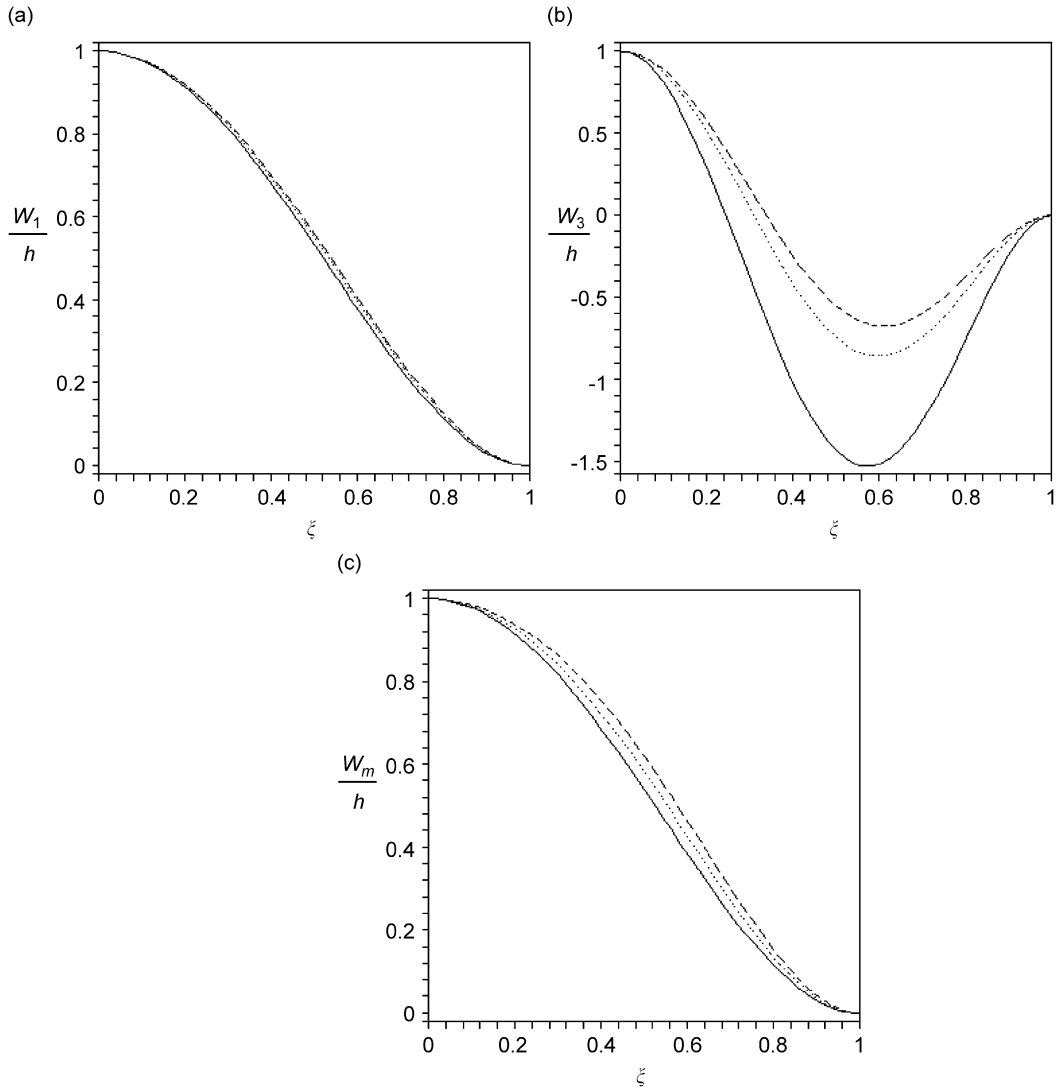

Fig. 12. Sections of shapes at $\eta = 0$, first main branch: (a) first harmonic; (b) third harmonic; and (c) shape of vibration at $t = 0$ s. Fundamental frequencies (—)$\omega/\omega_{\ell_1} = 1.05$, (···) $\omega/\omega_{\ell_1} = 1.2$, and (- - -) $\omega/\omega_{\ell_1} = 1.3$.

The first main branch is born from the second linear mode and, although the shape of vibration changes with the frequency, it remains very similar to the second linear mode along the complete period of vibration. The second main branch is related to the seventh mode of vibration and with the third harmonic. The shape changes with the frequency and amplitude of vibration, but remains similar to the shape of the seventh linear mode. The secondary branch links the bifurcation points of the two main branches. As one moves along the secondary branch, from the bifurcation point of the first main branch to the bifurcation point of the second main branch, the importance of first harmonic decreases while the importance of third harmonic increases. The shapes associated with the first and third harmonics of the first main branch and of the secondary branch, respectively, are presented in Fig. 15. The influence of the third harmonic on the secondary branch is obvious in Fig. 15(f).

4. Conclusion

A model to analyse geometrically nonlinear periodic vibrations of thin isotropic circular plates was presented. It is based on the principle of the virtual work, hierarchical basis functions and the harmonic

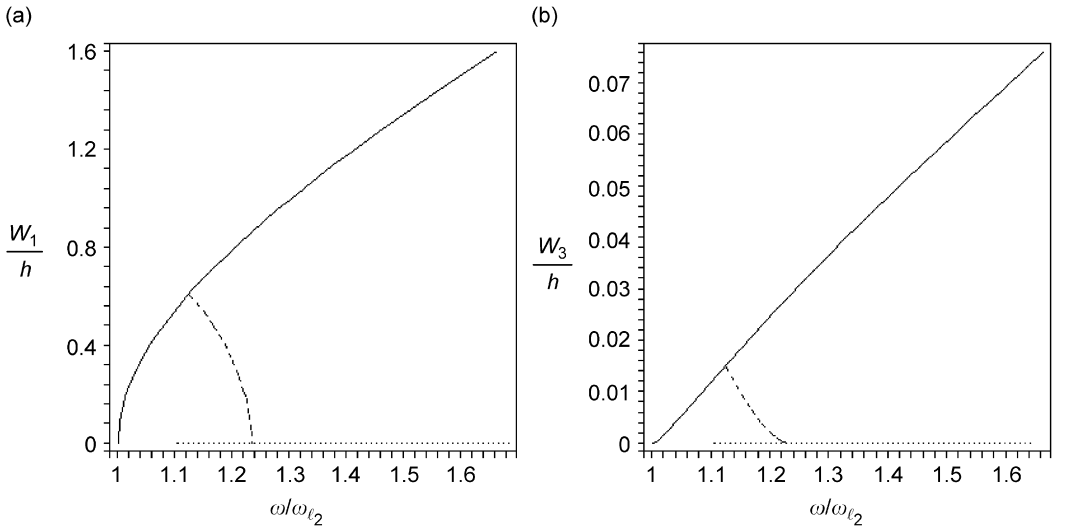

Fig. 13. Bifurcation diagram of the second mode at $(\xi, \eta) = (0.41, 0.5)$: (a) first harmonic and (b) third harmonic: (—) first main branch, (- - -) secondary branch, and (···) second main branch.

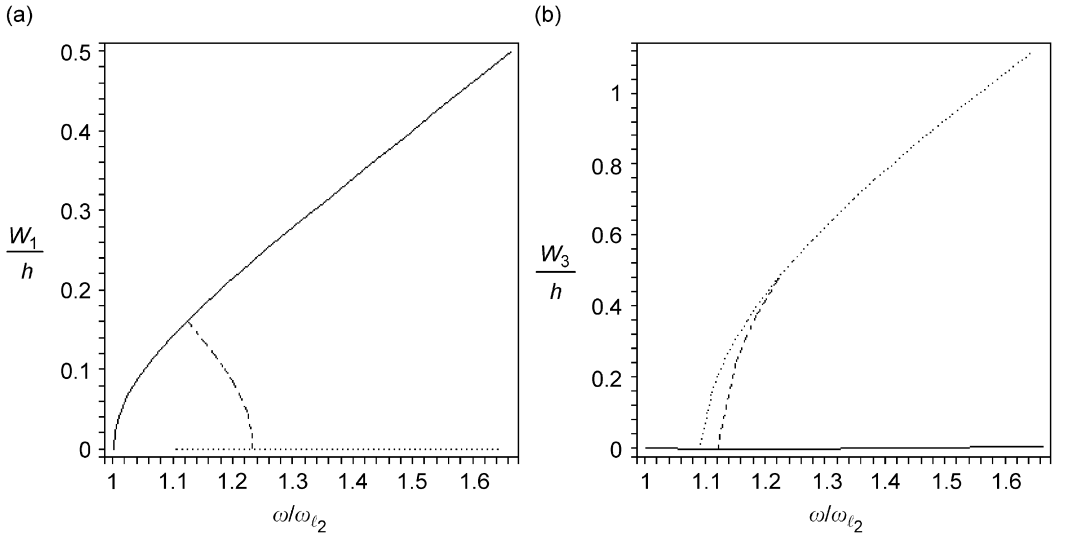

Fig. 14. Bifurcation diagram of the second mode at $(\xi, \eta) = (0.64, 0.875)$: (a) first harmonic, and (b) third harmonic; (—) first main branch, (- - -) secondary branch, and (···) second main branch.

balance method. It was shown that the convergence to accurate solutions with the number of shape functions and of harmonics is rapid, but also that a multi-degree-of-freedom model and more than one harmonic are often required for accuracy.

The first and second nonlinear modes of vibration were investigated and it was demonstrated that multimodal oscillations occur both in axisymmetric and in antisymmetric (in relation to the central axis) nonlinear modes. The bifurcations found occurred due to internal resonances between modes with different symmetry properties, leading to a loss of axisymmetry in the deformed shape of the plate. Coupling between modes with similar symmetry properties was also found—in our case between axisymmetric modes: it led to increasing curvature of the backbone curve, but not to secondary branches. Naturally, the coupling between modes and consequent excitation of higher harmonics leads to shapes of vibration that strongly change during the period of vibration.

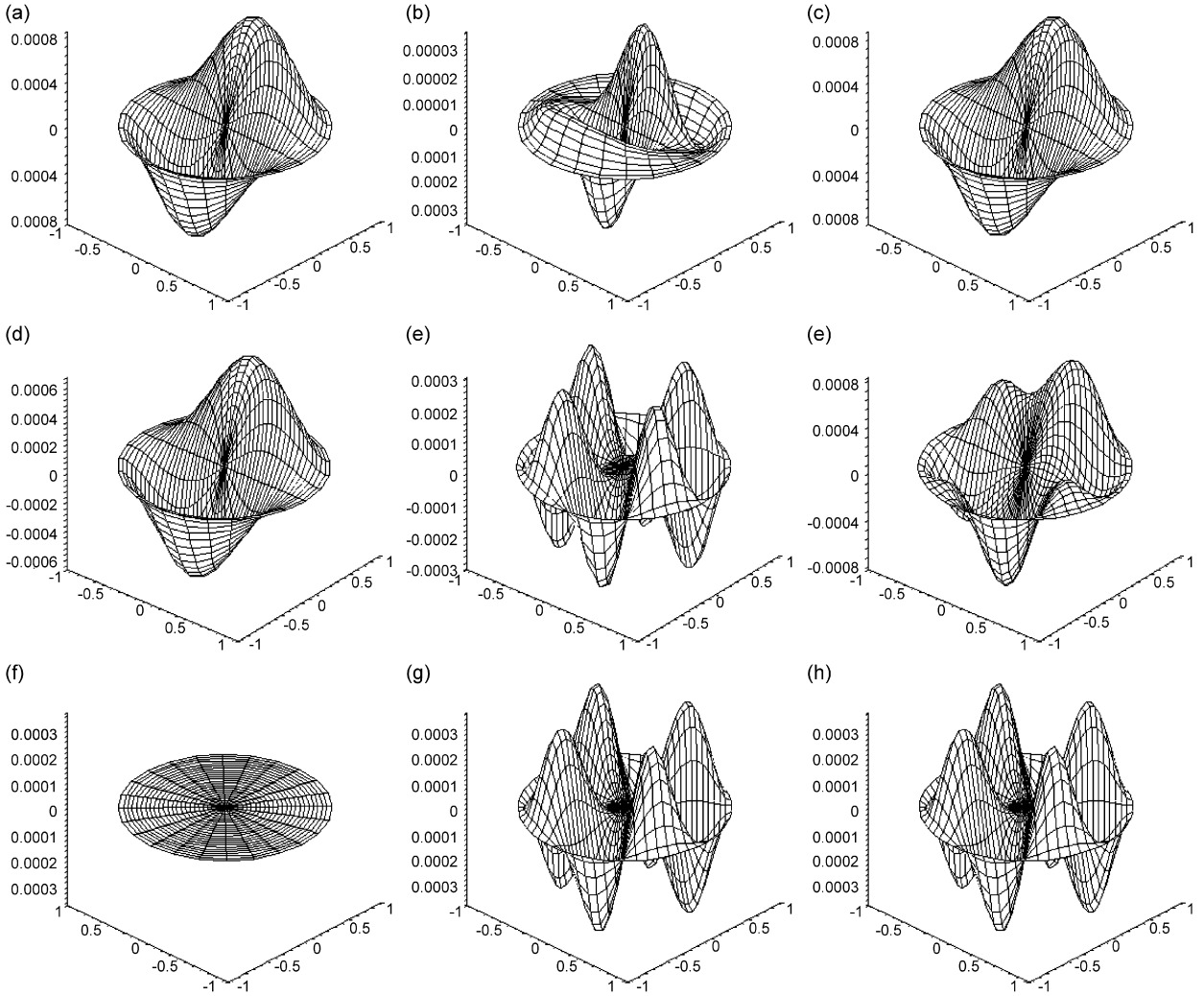

Fig. 15. Shapes of solutions on the three branches at frequency $\omega/\omega_{\ell_2} = 1.15$. First main branch: first harmonic (a), third harmonic (b), and total shape at $t = 0$ s (c). Secondary branch: first harmonic (d), third harmonic (e) and total shape at $t = 0$ s (f). Second main branch: first harmonic (g), third harmonic (h) and total shape at $t = 0$ s (i).

Travelling waves were not considered in the oscillation of this axisymmetric structure. Nevertheless, exactly the same methods should allow one to study the effect of travelling waves on the free nonlinear oscillations of circular plates, by inserting additional functions into the Fourier expansion of the displacements.

Appendix A. Shape functions

In this appendix the shape functions are presented. Since the boundaries are clamped and immovable—for other boundaries the following sets would be complemented with lower order polynomials—the in-plane radial and circumferential shape functions, both in the radial direction, are given by

$$g_{r-2}(\xi) = h_{r-2}(\xi) = \sum_{n=0}^{\mathrm{INT}(r/2)} \frac{(-1)^n (2r-2n-5)!!}{2^n n!(r-2n-1)!} \xi^{r-2n-1}, \quad r>2 \tag{A.1}$$

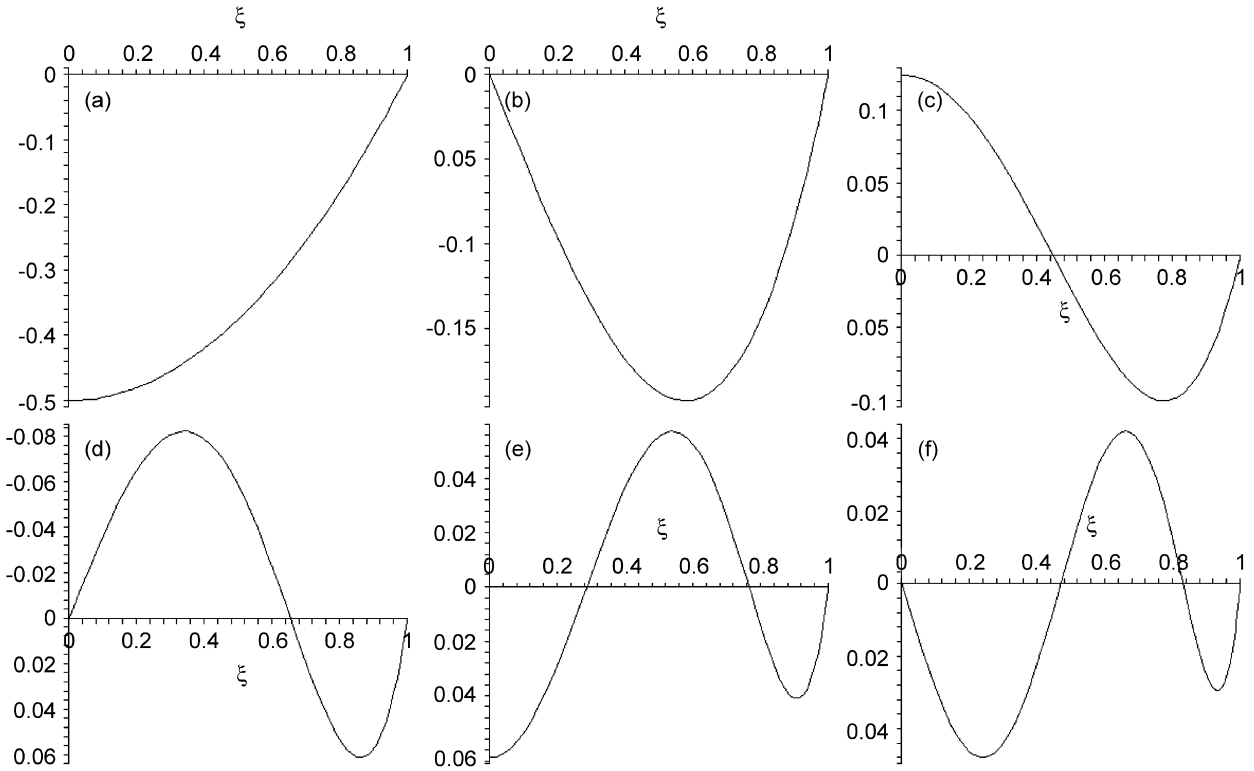

Fig. A1. In-plane radial and circumferential shape functions: $g_1(\xi)$ (a), $g_2(\xi)$ (b), $g_3(\xi)$ (c), $g_4(\xi)$ (d), $g_5(\xi)$ (e), $g_6(\xi)$ (f).

and the out-of-plane radial shape functions are given by

$$f_{r-4}(\xi) = \sum_{n=0}^{\mathrm{INT}(r/2)} \frac{(-1)^n (2r-2n-7)!!}{2^n n!(r-2n-1)!}\, \xi^{r-2n-1}, \quad r>4, \tag{A.2}$$

where $r!! = r(r-2)\ldots(2 \text{ or } 1)$, $0!! = (-1)!! = 1$ and $\mathrm{INT}(r/2)$ denotes the integer part of $r/2$. The argument ξ varies from 0 to 1. Figs. A1 and A2 show some of the functions $g(\xi)$ and $f(\xi)$, respectively.

The trigonometric sets of functions, employed as shape functions in the circumferential direction, are $gt_1(\eta) = ht_1(\eta) = ft_1(\eta) = 1$ and

$$ft_r(\eta) = \sin((r-1)\eta), \quad r>2, \tag{A.3}$$

$$gt_r(\eta) = \cos((r-1)\eta), \quad r>2, \tag{A.4}$$

$$ht_r(\eta) = \sin((r-1)\eta), \quad r>2. \tag{A.5}$$

Appendix B. Mass and stiffness matrices of time domain equations of motion

This appendix gives the mass, linear stiffness and nonlinear stiffness matrices of Eq. (12).

$\mathbf{M}_b$ and $\mathbf{K}_{1b}$ are given by

$$\mathbf{M}_{bp_o^2 \times p_o^2} = \rho h \int_\Omega \mathbf{N}^z \mathbf{N}^{z\mathrm{T}}\, \mathrm{d}\Omega, \tag{B.1}$$

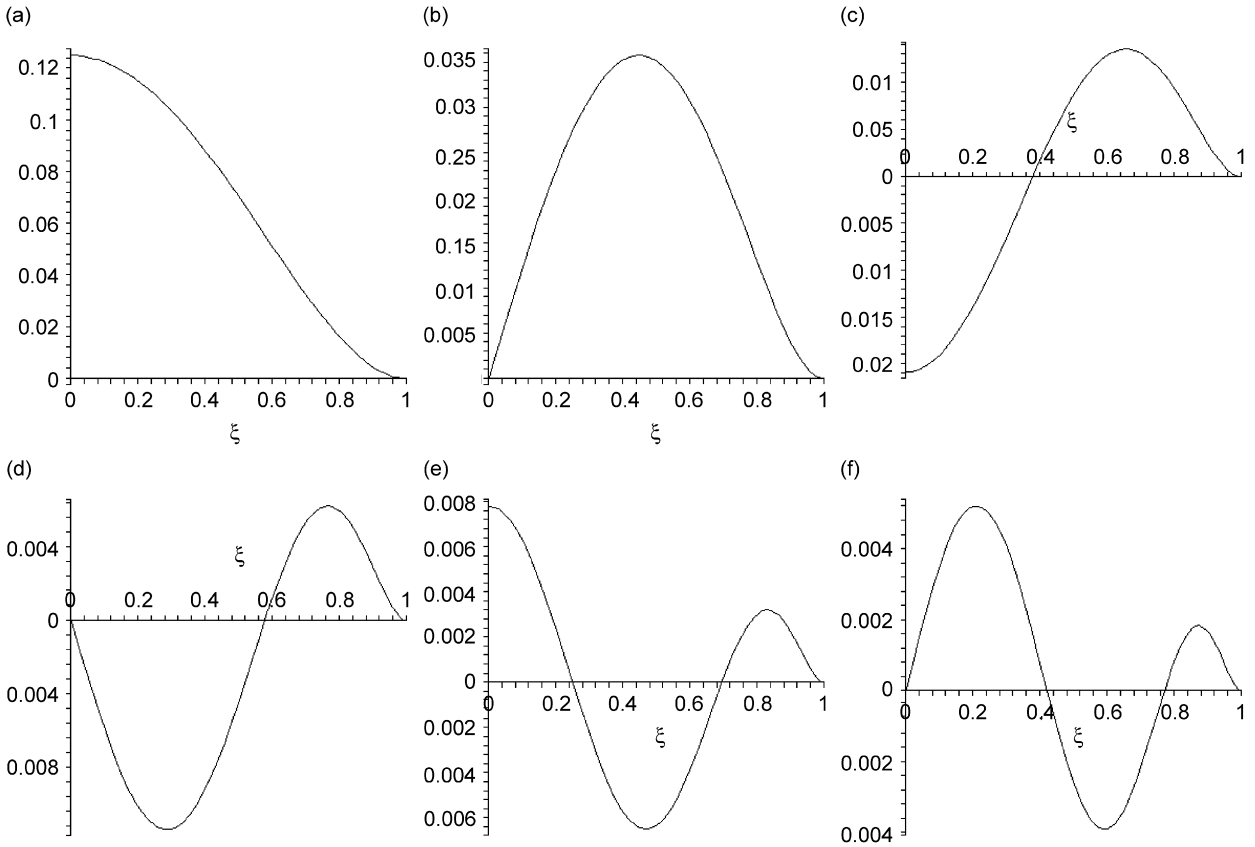

Fig. A1. Out-of-plane radial shape functions: f_1 (ξ) (a), f_2 (ξ) (b), f_3 (ξ) (c), f_4 (ξ) (d), f_5 (ξ) (e), and f_6 (ξ) (f).

$$K_{1bp_o^2\times p_o^2} = \int_\Omega \left[\frac{\partial^2 \mathbf{N}^z}{\partial r^2}\frac{1}{r}\frac{\partial \mathbf{N}^z}{\partial r} + \frac{1}{r^2}\frac{\partial^2 \mathbf{N}^z}{\partial \theta^2}\frac{2}{r}\frac{\partial^2 \mathbf{N}^z}{\partial r \partial \theta} - \frac{2}{r^2}\frac{\partial \mathbf{N}^z}{\partial \theta}\right] \times \begin{bmatrix} D_{11} & D_{12} & 0 \\ D_{12} & D_{22} & 0 \\ 0 & 0 & D_{66} \end{bmatrix} \begin{bmatrix} \dfrac{\partial^2 \mathbf{N}^{z\mathrm{T}}}{\partial r^2} \\ \dfrac{1}{r}\dfrac{\partial \mathbf{N}^{z\mathrm{T}}}{\partial r} + \dfrac{1}{r^2}\dfrac{\partial^2 \mathbf{N}^{z\mathrm{T}}}{\partial \theta^2} \\ \dfrac{2}{r}\dfrac{\partial^2 \mathbf{N}^{z\mathrm{T}}}{\partial r \partial \theta} - \dfrac{2}{r^2}\dfrac{\partial \mathbf{N}^{z\mathrm{T}}}{\partial \theta} \end{bmatrix} \mathrm{d}\Omega. \tag{B.2}$$

The indices in D_{ij} assume the values 1, 2 and 6, because the matrix **D**, defined by Eq. (11), results from a simplification of the generalized Hooke's law, which involves a 6×6 matrix [27]. The same applies to matrix **A** defined in Eq. (11).

The nonlinear stiffness matrices $\mathbf{K}_2$ and $\mathbf{K}_4$ are given by

$$\mathbf{K}_2 = \begin{bmatrix} \overline{\mathbf{U}} \\ \overline{\mathbf{V}} \end{bmatrix}_{2p_i^2\times p_o^2}, \tag{B.3}$$

where

$$\overline{\mathbf{U}} = \frac{1}{2}\int_{\Omega}\left[A_{11}\pi\frac{1}{R}\frac{\partial u_z}{\partial\xi}\frac{\partial \mathbf{N}^z}{\partial\xi}\frac{\partial \mathbf{N}^{z^{\mathrm{T}}}}{\partial\xi}\xi + A_{12}\pi\frac{1}{R}\frac{\partial u_z}{\partial\xi}N^z\frac{\partial \mathbf{N}^{z^{\mathrm{T}}}}{\partial\xi} + A_{12}\frac{1}{\pi}\frac{1}{R}\frac{1}{\xi}\frac{\partial u_z}{\partial\eta}\frac{\partial \mathbf{N}^z}{\partial\xi}\frac{\partial \mathbf{N}^{z^{\mathrm{T}}}}{\partial\eta} + A_{22}\frac{1}{\pi}\frac{1}{R}\frac{1}{\xi^2}\frac{\partial u_z}{\partial\eta}\mathbf{N}^z\frac{\partial \mathbf{N}^{z^{\mathrm{T}}}}{\partial\eta} + 2A_{66}\frac{1}{\pi}\frac{1}{R}\frac{1}{\xi}\frac{\partial u_z}{\partial\xi}\frac{\partial \mathbf{N}^z}{\partial\eta}\frac{\partial \mathbf{N}^{z^{\mathrm{T}}}}{\partial\eta}\right]\mathrm{d}\Omega, \tag{B.4}$$

$$\overline{\mathbf{V}} = \frac{1}{2}\int_{\Omega}\left[A_{12}\frac{1}{R}\frac{\partial u_z}{\partial\xi}\frac{\partial \mathbf{N}^{\theta}}{\partial\eta}\frac{\partial \mathbf{N}^{z^{\mathrm{T}}}}{\partial\xi} + A_{22}\frac{1}{\pi^2}\frac{1}{R}\frac{1}{\xi^2}\frac{\partial u_z}{\partial\eta}\frac{\partial \mathbf{N}^{\theta}}{\partial\eta}\frac{\partial \mathbf{N}^{z^{\mathrm{T}}}}{\partial\eta} + 2A_{66}\frac{1}{R}\frac{\partial u_z}{\partial\xi}\frac{\partial \mathbf{N}^{\theta}}{\partial\xi}\frac{\partial \mathbf{N}^{z^{\mathrm{T}}}}{\partial\eta} - 2A_{66}\frac{1}{R}\frac{1}{\xi}\frac{\partial u_z}{\partial\xi}\mathbf{N}^{\theta}\frac{\partial \mathbf{N}^{z^{\mathrm{T}}}}{\partial\eta}\right]\mathrm{d}\Omega \tag{B.5}$$

and

$$\begin{aligned}K_{4p_o^2\times p_o^2} = \frac{1}{2}\int_{\Omega}\Bigg[&A_{11}\pi\frac{1}{R^2}\left(\frac{\partial u_z}{\partial\xi}\right)^2\frac{\partial \mathbf{N}^z}{\partial\xi}\frac{\partial \mathbf{N}^{z^{\mathrm{T}}}}{\partial\xi}\xi + A_{12}\frac{1}{\pi}\frac{1}{R^2}\frac{1}{\xi}\left(\frac{\partial u_z}{\partial\xi}\right)^2\frac{\partial \mathbf{N}^z}{\partial\eta}\frac{\partial \mathbf{N}^{z^{\mathrm{T}}}}{\partial\eta}\\ &+ A_{12}\frac{1}{\pi}\frac{1}{R^2}\frac{1}{\xi}\left(\frac{\partial u_z}{\partial\eta}\right)^2\frac{\partial \mathbf{N}^z}{\partial\xi}\frac{\partial \mathbf{N}^{z^{\mathrm{T}}}}{\partial\xi} + A_{22}\frac{1}{\pi^3}\frac{1}{R^2}\frac{1}{\xi^3}\left(\frac{\partial u_z}{\partial\eta}\right)^2\frac{\partial \mathbf{N}^z}{\partial\eta}\frac{\partial \mathbf{N}^{z^{\mathrm{T}}}}{\partial\eta}\\ &+ A_{66}\frac{1}{\pi}\frac{1}{R^2}\frac{1}{\xi}\frac{\partial u_z}{\partial\xi}\frac{\partial u_z}{\partial\eta}\frac{\partial \mathbf{N}^z}{\partial\xi}\frac{\partial \mathbf{N}^{z^{\mathrm{T}}}}{\partial\eta} + A_{66}\frac{1}{\pi}\frac{1}{R^2}\frac{1}{\xi}\frac{\partial u_z}{\partial\eta}\frac{\partial u_z}{\partial\xi}\frac{\partial \mathbf{N}^z}{\partial\xi}\frac{\partial \mathbf{N}^{z^{\mathrm{T}}}}{\partial\eta}\\ &+ A_{66}\frac{1}{\pi}\frac{1}{R^2}\frac{1}{\xi}\frac{\partial u_z}{\partial\xi}\frac{\partial u_z}{\partial\eta}\frac{\partial \mathbf{N}^z}{\partial\eta}\frac{\partial \mathbf{N}^{z^{\mathrm{T}}}}{\partial\xi} + A_{66}\frac{1}{\pi}\frac{1}{R^2}\frac{1}{\xi}\frac{\partial u_z}{\partial\eta}\frac{\partial u_z}{\partial\xi}\frac{\partial \mathbf{N}^z}{\partial\eta}\frac{\partial \mathbf{N}^{z^{\mathrm{T}}}}{\partial\xi}\Bigg]\mathrm{d}\Omega.\end{aligned} \tag{B.6}$$

The in-plane linear stiffness matrix $\mathbf{K}_{1p}$ is given by

$$K_{1p2p_i^2\times 2p_i^2} = \int_{\Omega}\begin{bmatrix}\dfrac{\partial \mathbf{N}^r}{\partial r} & \dfrac{1}{r}\mathbf{N}^r & \dfrac{1}{r}\dfrac{\partial \mathbf{N}^r}{\partial\theta}\\ 0 & \dfrac{1}{r}\dfrac{\partial \mathbf{N}^{\theta}}{\partial\theta} & \dfrac{\partial \mathbf{N}^{\theta}}{\partial r} - \dfrac{1}{r}\mathbf{N}^{\theta}\end{bmatrix}\begin{bmatrix}A_{11} & A_{12} & 0\\ A_{12} & A_{22} & 0\\ 0 & 0 & A_{66}\end{bmatrix}\begin{bmatrix}\dfrac{\partial \mathbf{N}^{r^{\mathrm{T}}}}{\partial r} & 0\\ \dfrac{1}{r}\mathbf{N}^{r^{\mathrm{T}}} & \dfrac{1}{r}\dfrac{\partial \mathbf{N}^{\theta^{\mathrm{T}}}}{\partial\theta}\\ \dfrac{1}{r}\dfrac{\partial \mathbf{N}^{r^{\mathrm{T}}}}{\partial\theta} & \dfrac{\partial \mathbf{N}^{\theta^{\mathrm{T}}}}{\partial r} - \dfrac{1}{r}\mathbf{N}^{\theta^{\mathrm{T}}}\end{bmatrix}\mathrm{d}\Omega. \tag{B.7}$$

Appendix C. Harmonic balance equations of motion

In this appendix the frequency domain equations (16) are explicitly given for the particular case where three harmonics are used. The vector of generalized displacements is then defined as

$$\mathbf{w} = \begin{Bmatrix}\mathbf{w}_1\\ \mathbf{w}_3\\ \mathbf{w}_5\end{Bmatrix} \tag{C.1}$$

and the transverse displacement and the acceleration are given by

$$\mathbf{q}_z(t) = \mathbf{w}_1\cos(\omega t) + \mathbf{w}_3\cos(3\omega t) + \mathbf{w}_5\cos(5\omega t), \tag{C.2}$$

$$\ddot{\mathbf{q}}_z(t) = -\omega^2 \mathbf{w}_1 \cos(\omega t) - 9\omega^2 \mathbf{w}_3 \cos(3\omega t) - 25\omega^2 \mathbf{w}_5 \cos(5\omega t). \tag{C.3}$$

Substituting expressions (C.2) and (C.3) into equations of motion (16) and neglecting harmonics higher than $5\omega t$, the following frequency domain equations of motion are obtained:

$$\left(-\omega^2 \begin{bmatrix} \mathbf{M}_b & \mathbf{0} & \mathbf{0} \\ \mathbf{0} & 9\mathbf{M}_b & \mathbf{0} \\ \mathbf{0} & 0 & 25\mathbf{M}_b \end{bmatrix} + \begin{bmatrix} \mathbf{K}_{1b} & \mathbf{0} & \mathbf{0} \\ \mathbf{0} & \mathbf{K}_{1b} & \mathbf{0} \\ \mathbf{0} & \mathbf{0} & \mathbf{K}_{1b} \end{bmatrix} \right) \begin{Bmatrix} \mathbf{w}_1 \\ \mathbf{w}_3 \\ \mathbf{w}_5 \end{Bmatrix} + \begin{Bmatrix} \mathbf{F}_1 \\ \mathbf{F}_3 \\ \mathbf{F}_5 \end{Bmatrix} = \mathbf{0}. \tag{C.4}$$

The cubic nonlinear terms—$\mathbf{F}_1$, $\mathbf{F}_3$ and $\mathbf{F}_5$—are given by

$$\begin{Bmatrix} \mathbf{F}_1 \\ \mathbf{F}_3 \\ \mathbf{F}_5 \end{Bmatrix} = \mathbf{K}_{\mathrm{NL}} \begin{Bmatrix} \mathbf{w}_1 \\ \mathbf{w}_3 \\ \mathbf{w}_5 \end{Bmatrix}, \tag{C.5}$$

where the nonlinear stiffness matrix $\mathbf{K}_{\mathrm{NL}}$ is

$$\begin{aligned} \mathbf{K}_{\mathrm{NL}} = \frac{1}{4} \Bigg(& \begin{bmatrix} 3\mathbf{K}_{\mathrm{NL1}} & \mathbf{K}_{\mathrm{NL1}} & \mathbf{0} \\ \mathbf{K}_{\mathrm{NL1}} & 2\mathbf{K}_{\mathrm{NL1}} & \mathbf{K}_{\mathrm{NL1}} \\ \mathbf{0} & \mathbf{K}_{\mathrm{NL1}} & 2\mathbf{K}_{\mathrm{NL1}} \end{bmatrix} + 2 \begin{bmatrix} \mathbf{K}_{\mathrm{NL2}} & 2\mathbf{K}_{\mathrm{NL2}} & \mathbf{K}_{\mathrm{NL2}} \\ 2\mathbf{K}_{\mathrm{NL2}} & \mathbf{0} & \mathbf{K}_{\mathrm{NL2}} \\ \mathbf{K}_{\mathrm{NL2}} & \mathbf{K}_{\mathrm{NL2}} & \mathbf{0} \end{bmatrix} \\ & + 2 \begin{bmatrix} \mathbf{0} & \mathbf{K}_{\mathrm{NL3}} & 2\mathbf{K}_{\mathrm{NL3}} \\ \mathbf{K}_{\mathrm{NL3}} & \mathbf{K}_{\mathrm{NL3}} & \mathbf{0} \\ 2\mathbf{K}_{\mathrm{NL3}} & \mathbf{0} & \mathbf{0} \end{bmatrix} + \begin{bmatrix} 2\mathbf{K}_{\mathrm{NL4}} & \mathbf{0} & \mathbf{K}_{\mathrm{NL4}} \\ \mathbf{0} & 3\mathbf{K}_{\mathrm{NL4}} & \mathbf{0} \\ \mathbf{K}_{\mathrm{NL4}} & \mathbf{0} & \mathbf{K}_{\mathrm{NL4}} \end{bmatrix} \\ & + 2 \begin{bmatrix} \mathbf{K}_{\mathrm{NL5}} & \mathbf{K}_{\mathrm{NL5}} & \mathbf{0} \\ \mathbf{K}_{\mathrm{NL5}} & \mathbf{0} & 2\mathbf{K}_{\mathrm{NL5}} \\ \mathbf{0} & 2\mathbf{K}_{\mathrm{NL5}} & \mathbf{0} \end{bmatrix} + \begin{bmatrix} 2\mathbf{K}_{\mathrm{NL6}} & \mathbf{0} & \mathbf{0} \\ \mathbf{0} & 2\mathbf{K}_{\mathrm{NL6}} & \mathbf{0} \\ \mathbf{0} & \mathbf{0} & 3\mathbf{K}_{\mathrm{NL6}} \end{bmatrix} \Bigg). \end{aligned} \tag{C.6}$$

$\mathbf{K}_{\mathrm{NL}i}$ are of the form

$$\mathbf{K}_{\mathrm{NL}i}(\mathbf{w}_c, \mathbf{w}_c^*) = \mathbf{K}_4(\mathbf{w}_c, \mathbf{w}_c^*) - \mathbf{K}_2(\mathbf{w}_c)^{\mathrm{T}} \mathbf{K}_{1p}^{-1} \mathbf{K}_2(\mathbf{w}_c^*) - \mathbf{K}_2(\mathbf{w}_c^*)^{\mathrm{T}} \mathbf{K}_{1p}^{-1} \mathbf{K}_2(\mathbf{w}_c), \tag{C.7}$$

where $\mathbf{K}_4(\mathbf{w}_c, \mathbf{w}_c^*)$ means that this matrix is a quadratic function of vectors $\mathbf{w}_c$ and $\mathbf{w}_c$*. The following substitutions should be implemented in Eq. (C.7): $\mathbf{w}_c = \mathbf{w}_c^* = \mathbf{w}_1$ for $\mathbf{K}_{\mathrm{NL1}}$; $\mathbf{w}_c = \mathbf{w}_c^* = \mathbf{w}_3$ for $\mathbf{K}_{\mathrm{NL4}}$; $\mathbf{w}_c = \mathbf{w}_c^* = \mathbf{w}_5$ for $\mathbf{K}_{\mathrm{NL6}}$; $\mathbf{w}_c = \mathbf{w}_1$, $\mathbf{w}_c^* = \mathbf{w}_3$ for $\mathbf{K}_{\mathrm{NL2}}$; $\mathbf{w}_c = \mathbf{w}_1$, $\mathbf{w}_c^* = \mathbf{w}_5$ for $\mathbf{K}_{\mathrm{NL3}}$; $\mathbf{w}_c = \mathbf{w}_3$, $\mathbf{w}_c^* = \mathbf{w}_5$ for $\mathbf{K}_{\mathrm{NL5}}$.

Matrices $\mathbf{K}_{\mathrm{NL}i}$, $i = 1, \ldots, 6$ are symmetric.

References

[1] W. Szemplinska-Stupnicka, *The Behaviour of Nonlinear Vibrating Systems*, Kluwer Academic Publishers, Dordrecht, 1990.

[2] S. Sridhar, D.T. Mook, A.H. Nayfeh, Non-linear resonances in the forced responses of plates, part I: symmetric responses of circular plates, *Journal of Sound and Vibration* 41 (1975) 359–373.

[3] J. Hadian, A.H. Nayfeh, Modal interaction in circular plates, *Journal of Sound and Vibration* 142 (1990) 279–292.

[4] C.-F. Liu, G.-T. Chen, Geometrically nonlinear axisymmetric vibrations of polar orthotropic circular plates, *International Journal of Mechanical Sciences* 3 (1996) 325–333.

[5] M. Haterbouch, Effects of the Geometrically Non-linearity on the Free and Forced Response of Clamped and Simply Supported Circular Plates, PhD Thesis, Université Mohammed V-Agdal, Rabat, 2003.

[6] M. Haterbouch, R. Benamar, The effects of large vibration amplitudes on the axisymmetric mode shapes and natural frequencies of clamped thin isotropic circular plates. Part I: iterative and explicit analytical solution for non-linear transverse vibrations, *Journal of Sound and Vibration* 265 (2003) 123–154.

[7] M. Haterbouch, R. Benamar, The effects of large vibration amplitudes on the axisymmetric mode shapes and natural frequencies of clamped thin isotropic circular plates. Part II: iterative and explicit analytical solution for non-linear coupled transverse and in-plane vibrations, *Journal of Sound and Vibration* 277 (2004) 1–30.

[8] M. Haterbouch, R. Benamar, Geometrically nonlinear free vibrations of simply supported isotropic thin circular plates, *Journal of Sound and Vibration* 280 (2005) 903–924.

[9] K. Kanaka Raju, G. Venkateswara Rao, Axisymmetric vibrations of circular plates including the effects of geometric non-linearity, shear deformation and rotary inertia, *Journal of Sound and Vibration* 47 (1976) 179–184.
[10] M. Sathyamoorthy, Influence of transverse shear and rotatory inertia on nonlinear vibrations of circular plates, *Computers and Structures* 60 (1996) 613–618.
[11] S. Sridhar, D.T. Mook, A.H. Nayfeh, Non-linear resonances in the forced responses of plates, part II: asymmetric responses of circular plates, *Journal of Sound and Vibration* 59 (1978) 159–170.
[12] M.H. Yeo, W.K. Lee, Corrected solvability conditions for non-linear asymmetric vibrations of a circular plate, *Journal of Sound and Vibration* 257 (2002) 653–665.
[13] W.K. Lee, M.H. Yeo, Non-linear interactions in asymmetric vibrations of a circular plate, *Journal of Sound and Vibration* 263 (2003) 1017–1030.
[14] C. Touzé, O. Thomas, A. Caigne, Asymmetric non-linear forced vibrations of free-edge circular plates. Part 1: theory, *Journal of Sound and Vibration* 258 (2002) 649–676.
[15] O. Thomas, C. Touzé, A. Chaigne, Asymmetric non-linear forced vibrations of free-edge circular plates. Part II: experiments, *Journal of Sound and Vibration* 265 (2003) 1075–1101.
[16] N.S. Bardell, Free vibration analysis of a flat plate using the hierarchical finite element method, *Journal of Sound and Vibration* 151 (1991) 263–289.
[17] W. Han, M. Petyt, Geometrically nonlinear vibration analysis of thin, rectangular plates using the hierarchical finite element method—I: the fundamental mode of isotropic plates, *Computers & Structures* 63 (1997) 295–308.
[18] P. Ribeiro, Geometrical Non-linear Vibration of Beams and Plates by the Hierarchical Finite Element Method, PhD Thesis, University of Southampton, 1998.
[19] P. Ribeiro, M. Petyt, Non-linear vibration of plates by the hierarchical finite element and continuation methods, *International Journal of Mechanical Sciences* 41 (1999) 437–459.
[20] P. Ribeiro, M. Petyt, Non-linear free vibration of isotropic plates with internal resonance, *International Journal of Non-linear Mechanics* 35 (2000) 263–278.
[21] P. Ribeiro, Hierarchical finite element analyses of geometrically non-linear vibration of beams and plane frames, *Journal of Sound and Vibration* 246 (2001) 225–244.
[22] C. Liu, Y. Lee, Finite element analysis of three-dimensional vibrations of circular and annular plates, *Journal of Sound and Vibration* 233 (2000) 63–80.
[23] R. Lewandowski, Non-linear free vibration of beams by the finite element and continuation methods, *Journal of Sound and Vibration* 170 (1994) 577–593.
[24] E. Riks, An incremental approach to the solution of snapping and buckling problems, *International Journal of and Solids Structures* 15 (1979) 529–551.
[25] A. Leissa, Vibration of plates, NASA SP-169, Office of Technology Utilization, Washington, 1969, re-issued 1993 by the Acoustical Society of America.
[26] T.D. Burton, M.N. Hamdan, On the calculation of non-linear normal modes in continuous systems, *Journal of Sound and Vibration* 197 (1996) 117–130.
[27] C.Y. Chia, *Non-linear Analysis of Plates*, McGraw-Hill, New York, 1980.